ASTE CO(3–2) Observations of the Southern Barred Spiral Galaxy NGC 986: a Large Gaseous Bar Filled with Dense Molecular Medium

Kotaro KOHNO,[1] Tomoka TOSAKI,[2] Rie MIURA,[3,4] Kazuyuki MURAOKA,[1] Tsuyoshi SAWADA,[2] Kouichiro NAKANISHI,[2] Nario KUNO,[2] Takeshi SAKAI,[2] Kazuo SORAI,[5] Kazuhisa KAMEGAI,[1] Kunihiko TANAKA,[1] Takeshi OKUDA,[1*] Akira ENDO,[1,3] Bunyo HATSUKADE,[1] Masahiro SAMESHIMA,[1] Hajime EZAWA,[3] Seiichi SAKAMOTO,[3†] Takeshi KAMAZAKI,[3] Nobuyuki YAMAGUCHI,[3] Juan CORTES,[3,6] Yoichi TAMURA,[3,4] Masayuki FUKUHARA,[3,4] Daisuke IONO,[3‡] and Ryohei KAWABE,[3]

[1]*Institute of Astronomy, The University of Tokyo, 2-21-1 Osawa, Mitaka, Tokyo 181-0015*
(KK) kkohno@ioa.s.u-tokyo.ac.jp

[2]*Nobeyama Radio Observatory, Minamimaki, Minamisaku, Nagano 384-1805*

[3]*National Astronomical Observatory of Japan, 2-21-1 Osawa, Mitaka, Tokyo 181-8588*

[4]*Department of Astronomy, The University of Tokyo, Hongo, Bunkyo-ku, Tokyo 113-0033*

[5]*Division of Physics, Graduate School of Science, Hokkaido University, Sapporo 060-0810*

[6]*Departamento de Astronomia, Universidad de Chile, Casilla 36-D, Santiago, Chile*

[*]*Present address is National Astronomical Observatory of Japan,*
2-21-1 Osawa, Mitaka, Tokyo 181-8588

[†]*Present address is Institute of Space and Astronautical Science,*
Japan Aerospace Exploration Agency, 3-1-1 Yoshinodai, Sagamihara, Kanagawa 229-8510

[‡]*Present address is Institute of Astronomy, The University of Tokyo,*
2-21-1 Osawa, Mitaka, Tokyo 181-0015

(Received ; accepted)

Abstract

We present CO(3–2) emission observations toward the $3' \times 3'$ (or 20×20 kpc at a distance of 23 Mpc) region of the southern barred spiral galaxy NGC 986 using the Atacama Submillimeter Telescope Experiment (ASTE). This effort is a part of our on-going extragalactic CO(3–2) imaging project ADIoS (ASTE Dense gas Imaging of Spiral galaxies). Our CO(3–2) image revealed the presence of a large (the major axis is 14 kpc in total length) gaseous bar filled with dense molecular medium along the dark lanes observed in optical images. This is the largest "dense-gas rich bar" known to date. The dense gas bar discovered in NGC 986 could be a huge reservoir of possible "fuel" for future starbursts in the central region, and we suggest that the star formation in the central region of NGC 986 could still be in a growing phase. We

1

found a good spatial coincidence between the overall distributions of dense molecular gas traced by CO(3–2) and the massive star formation depicted by Hα. The global CO(3–2) luminosity $L'_{\mathrm{CO(3-2)}}$ of NGC 986 was determined to be $(5.4 \pm 1.1) \times 10^8$ K km s^{-1} pc^2. The CO(3–2)/CO(1–0) integrated intensity ratio was found to be 0.60 $\pm$ 0.13 at a spatial resolution of $44''$ or 5 kpc, and a CO(3–2)/CO(2–1) ratio was 0.67 ± 0.14 at a beam size of $\sim 25''$ or ~ 2.8 kpc. These line ratios suggest moderate excitation conditions of CO lines ($n_{\mathrm{H_2}} \sim 10^{3-4}$ cm^{-3}) in the central a few kpc region of NGC 986.

Key words: galaxies: ISM —galaxies: individual (NGC 986) —galaxies: starburst —galaxies: structure —submillimeter

1. Introduction

The dense molecular medium is one of the indispensable components to understand the star formation law in galaxies. This is because stars are formed from dense molecular cores, not from the diffuse envelopes of giant molecular clouds (GMCs). In fact, extragalactic observations of millimeter-wave HCN(1–0) emission, which is a tracer of high density molecular medium ($n_{\mathrm{H_2}} \sim 10^5$ cm^{-3}) due to its high permanent dipole moment ($\mu = 3.0$ Debye), demonstrate that the correlation between HCN(1–0) and far-infrared (FIR) luminosities is better than that between CO(1–0) and FIR luminosities (Solomon et al. 1992; Gao & Solomon 2004a). However, the weakness of HCN emission (typically 1/10 in T_{b} of CO in the central regions of galaxies, and 1/30 - 1/50 of CO in the disk regions of the Galaxy (Helfer & Blitz 1997b) and galaxies (Helfer & Blitz 1993; Kohno et al. 1996; Kohno et al. 1999; Kohno et al. 2003; Gao & Solomon 2004b) often prevents us from obtaining large-scale maps of the dense molecular medium through HCN observations.

In order to understand the global distribution of dense molecular medium in galaxies, we have conducted an extragalactic CO(3–2) imaging survey of nearby spiral galaxies, ADIoS (ASTE Dense gas Imaging of Spiral galaxies). The current sample galaxies of the ADIoS project are listed in Table 1. The submillimeter-wave CO(3–2) emission is another tracer of dense gas because its Einstein A coefficient is proportional to ν^3; therefore, the critical density of CO(3–2) emission is higher than that of CO(1–0) by a factor of $\sim 3^3$, i.e., $n_{\mathrm{H_2}} \sim 10^4$ cm^{-3}.

The Atacama Submillimeter Telescope Experiment (ASTE; Ezawa et al. 2004), a new project to operate a 10 m telescope in the Atacama Desert of northern Chile, provides us with an ideal opportunity to generate large-scale maps of CO(3–2) emission because of the high beam efficiency of the telescope, a low system noise temperature due to the good receiver system and atmospheric conditions at the site, and its efficient on-the-fly (OTF) mapping capability (Sawada et al. 2008).

Here, we present the CO(3–2) images of the southern CO luminous spiral galaxy NGC

986 as the initial result of the ADIoS project by using OTF mapping. NGC 986 is a nearby ($D = 23.2$ Mpc; Tully 1988) barred spiral galaxy accompanied with an outer pseudo ring (i.e., (R$'_1$)SB(rs)b, Buta 1995). It is a member of the IRAS bright galaxy sample (Sanders et al. 2003); however, its FIR luminosity is rather moderate ($L_{\mathrm{FIR}} = 3.5 \times 10^{10} L_\odot$) [1]. The nucleus is classified as HII (Veron-Cetty & Veron 1986), and extended massive star forming regions along the bar have been imaged in Hα (Hameed & Devereux 1999; Koopmann & Kenney 2006) and mid-infrared continuum (Dale et al. 2000; see also Förster Schreiber et al. 2004). The central region of NGC 986 is very rich in interstellar medium (ISM), and there are many reports on the observations of various atomic lines in the near-infrared (NIR) to FIR regions (Kawara et al. 1987; Kawara et al. 1989; Thornley et al. 2000; Malhotra et al. 2001) and molecular lines at millimeter wavelengths (Aalto et al. 1991; Aalto et al. 1995; Elfhag et al. 1996). In fact, NGC 986 is one of the brightest galaxies in terms of CO(1–0) emission in the sample of Elfhag et al. (1996), thereby rendering this galaxy as an ideal target for our ADIoS project. It should be noted that all the previous CO observations of NGC 986 were conducted just toward the central position and no CO map of NGC 986 has been published yet.

2. Observations and Data Reduction

The CO(3–2) observations towards NGC 986 were conducted using the ASTE on September 14 and 15, 2006. The total time for observation was 10 hours. The mapped region was $3' \times 3'$ (20×20 kpc), covering almost the entire region of the optical disk. The half-power beam width (HPBW) of the ASTE 10 m dish is $22''$ at this frequency; this corresponds to 2.5 kpc at a distance of 23 Mpc.

The front end was a cartridge-type cooled SIS mixer receiver for the DSB operation, SC345 (Kohno 2005; Muraoka et al. 2007). The back end was a digital autocorrelator system, MAC (Sorai et al. 2000b), which is comprised of four banks of a 512 MHz wide spectrometer with 1024 spectral channels each. This arrangement provided a velocity coverage of 440 km s^{-1} with a velocity resolution of 0.43 km s^{-1}. The observations were made remotely from an ASTE operation room of NRO using a network observation system N-COSMOS3 developed by the National Astronomical Observatory of Japan (NAOJ) (Kamazaki et al. 2005).

OTF mapping was performed along two different directions (i.e., scans along the RA and Decl. directions), and these two data sets were co-added by the Basket-weave method (Emerson & Graeve 1988) in order to remove effects of scanning noise. At the end of each OTF scan, an off-source position ($5'$ offset from the map center in the azimuth) was observed to subtract sky emission.

We observed the CO(3–2) emission of O-Ceti (Mira) every 2 hours in order to monitor the stabilities of the pointing accuracy and main beam efficiency (η_{mb}) of the ASTE 10 m dish.

---

[1] This L_{FIR} is rescaled to the value for the distance we assumed here.

The pointing accuracy was found to be better than $\sim 2''$ r.m.s. and η_{mb} was estimated to be 0.6 during the observing runs. The absolute error of the CO(3–2) amplitude scale was $\sim \pm$ 20 %, mainly due to the variation in the beam efficiency.

The data reduction was made using the software package *NOSTAR*, which comprises tools for OTF data analysis developed by NAOJ (Sawada et al. 2008). The raw data were regridded to $8''$ per pixel, giving an effective spatial resolution of approximately $25''$ (or 2.8 kpc). Linear baselines were removed from the spectra. We binned the adjacent channels to a velocity resolution of 10 km s^{-1} at the frequency of CO(3–2). The resultant r.m.s. noise level (1 σ) was around 25 mK on the T_{mb} scale or 1.5 Jy beam^{-1} at a beam size of $25''$ (HPBW). It is noteworthy that at this frequency and beam size, a brightness temperature of 1 K on the T_{mb} scale corresponds to a flux density of 60.7 Jy beam^{-1} .

After producing a 3D data cube, we analyzed it using AIPS. The 0th and 1st moment maps were computed using a clip level of 50 mK (or 2 σ) by the AIPS task MOMNT. A three-channel Hanning smoothing along the velocity axis was applied in order to mitigate the contribution from noise.

3. Results

3.1. Channel maps, spectrum, and moment maps

The derived velocity channel maps of CO(3–2) emission in NGC 986 are displayed in figure 1. We find a strong concentration of CO emission toward the center with a large veocity width (from 1865 to 2015 km s^{-1}; see also the CO(3–2) spectrum at the central position in figure 2); however, the extended emission along the SW to NE direction in some velocity channels (from 1925 to 1985 km s^{-1}) is also evident.

The 0th and 1st moment maps, i.e., a velocity integrated intensity map and an intensity-weighted mean velocity map, respectively, are shown in figure 3. The peak position of CO(3–2) emission, fitted by the AIPS task IMFIT, coincides well with the NIR peak within an accuracy of less than $1''$.

In addition to the strong CO condensation at the center, we can clearly see extensions of the CO emission along the bar and outer spiral arms, as observed in the R-band and Hα images (Hameed & Devereux 1999). The major axis of this gaseous bar seen in CO(3–2) emission is ~ 2 arcmin or 14 kpc. The nature of the gaseous bar will be discussed in section 4.

3.2. Spatial coincidence between CO(3–2) and Hα emissions

In figure 3(d), we find a good spatial coincidence between the overall distributions of dense molecular gas traced by CO(3–2) and the massive star formation depicted by Hα at a spatial scale of ~ 3 kpc. This is expected from the recent CO(3–2) observations that demonstrate a tight correlation between CO(3–2) and Hα luminosities (Komugi et al. 2007) thereby indicating an intimate association of the dense molecular medium with massive star formation

4

(see also Yao et al. 2003). It is intriguing to study whether CO(3–2) emission also shows a *better* spatial coincidence with the massive star forming regions as compared to the low-density gas traced by the CO(1–0) emission. In fact, previous surveys of CO(3-2) and CO(1-0) lines toward the centers of star-forming galaxies suggest that CO(3-2) luminosities show a *tighter* correlation with star-formation rates (traced by Hα or FIR) than that of CO(1-0) luminosities (Komugi et al. 2007; Yao et al. 2003). Future high-resolution low-J CO observations might be able to address this issue.

3.3. Global CO(3–2) luminosity

The total CO(3–2) flux of NGC 986 was measured using the AIPS task TVSTAT. The mean CO(3–2) intensity was 4.5 K km s^{-1} averaged over 147 pixels or 1.2×10^8 pc^2. This gives a global CO(3–2) luminosity $L'_{\mathrm{CO(3-2)}}$ of $(5.4 \pm 1.1) \times 10^8$ in the unit of K km s^{-1} pc^2. Note that the quoted error represents the systematic uncertainty, mainly due to the accuracy of main beam efficiency ($\pm$ 20 %). The derived CO(3–2) luminosity of NGC 986 is comparable with that of inner $5' \times 5'$ region of M 83 (Muraoka et al. 2007).

3.4. CO(3–2)/CO(1–0) and CO(3–2)/CO(2–1) intensity ratios

We compared the CO(3–2) intensity we obtained at the central position with the existing CO(1–0) (Aalto et al. 1991; Elfhag et al. 1996) and CO(2–1) (Aalto et al. 1995) measurements. All the previous observations were made using the SEST 15 m telescope. In order to compare our CO(3–2) data with the low-resolution (43″ or 44″ resolution) CO(1–0) intensities, we convolved our CO(3–2) cube to the same spatial resolution (44″). The SEST CO(2–1) observations had a beam size similar to that of the ASTE CO(3–2) observations, and no correction was made in the derivation of a CO(3–2)/CO(2–1) line ratio. The integrated intensities of various CO transitions were then summarized (in Table 3).

The CO(3–2)/CO(1–0) integrated intensity ratio $R_{3-2/1-0}$ was 0.60 ± 0.13 at a spatial resolution of 44″ or 5 kpc, and the CO(3–2)/CO(2–1) ratio $R_{3-2/2-1}$ was 0.67 ± 0.14 for a beam size of ~25″ or ~2.8 kpc.

The observed $R_{3-2/1-0}$ value, ~0.6, is greater than those of the GMCs in the disk regions of the Milky Way (~ 0.4, Sanders et al. 1993; ~ 0.5, Oka et al. 2007) and M 31 (~ 0.3, Tosaki et al. 2007a). Elliptical galaxies with very low-level star formation also show low ratios (~ 0.4, Vila-Vilaró et al. 2003). Similar $R_{3-2/1-0}$ values are reported in the inner a few kpc region of M 83 (0.6–0.7, Muraoka et al. 2007) and infrared luminous galaxies (~ 0.6, Mauersberger et al. 1999; Yao et al. 2003), and dwarf starburst galaxies (~ 0.6, Meier et al. 2001). Some of nearby starburst galaxies or giant HII regions in galaxies exibit high $R_{3-2/1-0}$ values close to unity (Devereux et al. 1994; Dumke et al. 2001; Tosaki et al. 2007b). The central molecular zone of the Milky Way (a size of ~ 200 pc) also shows high $R_{3-2/1-0}$ ratio (~ 0.9, Oka et al. 2007). Note that the apperture sizes/beam sizes of these line ratio measurements are a few 100 to a few kpc scales, and therefore mixture of multiple ISM components must be observed.

The observed line ratios in NGC 986 suggest a moderate excitation condition of the CO lines within the central a few kpc region of this galaxy. For instance, $R_{3-2/2-1}$ of 0.7 suggest that the mean gas density n_{H_2} averaged over a $\sim$2.8 kpc region in diameter is within a range of 10^3 to 10^4 cm^{-3} based on an LVG model by assuming a kinetic temperature of 30 K (see Fig. 8 of Hafok & Stutzki 2003 for instance). Additional mapping observations of low-J CO lines will be essential to determine the spatial distribution of CO line ratios, allowing us to impose constraints on the physical properties of ISM for various positions in NGC 986.

3.5. Molecular gas mass

From our global CO(3–2) luminosity of NGC 986, the total molecular gas mass was estimated to be

$$M(H_2) = 2.6 \times 10^9 \left(\frac{\alpha_{CO}}{2.9 \ M_\odot (\text{K km s}^{-1} \ \text{pc}^2)^{-1}} \right) \left(\frac{R_{3-2/1-0}}{0.6} \right)^{-1} M_\odot. \tag{1}$$

Here, we adopted a Galactic CO(1–0)-to-H$_2$ conversion factor $\alpha_{CO} = 2.9 \ M_\odot$ (K km s^{-1} pc^2)$^{-1}$ (equivalent to $X_{CO} = 1.8 \times 10^{20}$ cm^{-2} (K km s^{-1})$^{-1}$, Dame et al. 2001)) and a CO(3–2)/CO(1–0) ratio $R_{3-2/1-0}$ of 0.6 (see subsection 3.4). This molecular gas mass is comparable to those in nearby gas-rich spiral galaxies such as M 51 ($6 \times 10^9 \ M_\odot$, Kuno et al. 1995) and M 83 (3–4 $\times 10^9 \ M_\odot$, Crosthwaite et al. 2002; Lundgren et al. 2004).

3.6. Star formation efficiency

The star formation efficiency (SFE), a star formation rate per unit gas mass, is then $L_{FIR}/M(H_2) = 14 \ L_\odot/M_\odot$. Note that both L_{FIR} and $M(H_2)$ were measured over the almost entire region of this galaxy (i.e., determined for the same area). This SFE in NGC 986 is indeed close to the SFEs of nearby isolated or field spiral galaxies, $L_{FIR}/M(H_2) \sim 3 - 5 \ L_\odot/M_\odot$ (Young et al. 1996). Note that Young et al. (1996) assumed an $X_{CO} = 2.8 \times 10^{20}$ cm^{-2} (K km s^{-1})$^{-1}$; if we recalibrate the SFEs using the same X_{CO} value as for NGC 986 (Dame et al. 2001), the SFEs for nearby isolated or field spirals will be $\sim 5 - 8 \ L_\odot/M_\odot$, which are more closer to that of NGC 986. On the other hand, the observed SFE in NGC 986 is much lower than those in local IR luminous galaxies, $L_{FIR}/M(H_2) \sim 120 \ L_\odot/M_\odot$ (a mean value computed from Table 2 of Yao et al. 2003). Here Yao et al. (2003) determined the X_{CO} of their sample to be 2.7×10^{19} cm^{-2} (K km s^{-1})$^{-1}$, about 1/10 of a typical Galactic CO-to-H$_2$ conversion factor.

Another direct quantity related to SFE is the FIR to CO(3–2) luminosity ratio $L_{FIR}/L'_{CO(3-2)}$, a measure of star formation rate per unit dense-gas mass. We find the $L_{FIR}/L'_{CO(3-2)}$ ratio of 67 $L_\odot/$(K km s^{-1} pc^2) in NGC 986. This is comparable to the $L_{FIR}/L'_{CO(3-2)}$ values found in local IR luminous galaxies, a few 10 $L_\odot/$(K km s^{-1} pc^2), that was calculated from Yao et al. 2003, yet still much smaller than Ultra/Hyper luminous IR galaxies in the early universe, such as the submillimeter galaxy MIPS J142824.0+352619 at $z = 1.3$, showing the $L_{FIR}/L'_{CO(3-2)}$ of $264 \pm 84 \ L_\odot/$(K km s^{-1} pc^2) (Iono et al. 2006).

6

3.7. Kinematics of dense molecular gas

We find a clear velocity gradient in the mean-velocity map (figure 3(b)). We therefore determined the kinematical parameters of the gas disk, i.e., the dynamical center, systemic velocity, the position angle of the major axis, and inclination angle of the disk by a least-squares fitting of the intensity-weighted isovelocity field to a circular rotation model. The AIPS task GAL was used for this analysis. The fitting was made within a radius of $1'$, where the observed velocity field seems to be dominated by a circular motion. In general, strong non-circular motions are expected in the central regions of barred galaxies, but it is not clear in our map; it could be probably due to the insufficient spatial resolution of our observations.

The dynamical center coincides well with the nucleus position determined by the NIR (2MASS) peak within an error of a few arcsec. The systemic velocity (LSR) was determined to be 1942 ± 10 km s^{-1} (or corresponding to a heliocentric velocity of 1957 ± 10 km s^{-1}). This agrees well with the CO(1–0) result (Elfhag et al. 1996) and is close to the HI velocity measurement (Roth et al. 1994). See Table 2 for comparison. The position angle of the major axis and the inclination angle of the disk were estimated to be $127°$ (from north to east) and $37°$ ($0°$ is face-on), respectively. These kinematically determined angles are consistent with the previously reported isophotal values based on optical and NIR broad band images of NGC 986 (Tully 1988; de Vaucouleurs et al. 1991; Jarrett et al. 2003). The comparison of these angles is shown in Table 2.

A position-to-velocity map (PV map) was generated along the determined major axis (P.A. = $53°$), as shown in figure 4. The velocity gradient along the major axis was found to be ~ 10 km s^{-1} arcsec^{-1} from the figure; however, but we require much higher angular resolution measurements of the PV map, using SMA for instance, in order to determine the inner rotation curve of NGC 986.

4. Discussion: a large ($\sim$14 kpc) gaseous bar filled with dense molecular medium

Our CO(3–2) image revealed the presence of a large (~ 14 kpc) gaseous bar filled with dense molecular medium along the dark lanes observed in the optical images. This is the largest "dense-gas rich bar" known to date; previous large scale CO(3–2) imaging observations of nearby galaxies revealed that a centrally concentrated CO(3–2) morphology of around a few kpc scale is very common (Hurt et al. 1993; Mauersberger et al. 1996; Israel & Baas 2001; Dumke et al. 2001; Israel & Baas 2003). Some gas-rich barred spiral galaxies such as NGC 6946 (Israel & Baas 2001; Walsh et al. 2002), and M 83 (Israel & Baas 2001; Bayet et al. 2006; Muraoka et al. 2007), exhibit a wide spread CO(3–2) emission over the disk region; however, no such instances of large ($\sim$10 kpc scale) dense molecular gas bar have been reported thus far. Therefore, it is indeed a surprise to discover a 14 kpc long gaseous bar observed in CO(3–2) emission among nearby spiral galaxies. Note that this is even true in the case of bars

observed in low-J CO lines. Some galaxies such as NGC 1530 (Downes et al. 1996), UGC 2855 (Hüttemeister et al. 1999), and NGC 7479 (Sempere et al. 1995) do exhibit a continuous bar, observed in CO(1–0) and/or CO(2–1) emission, with a length of ∼10 kpc; however, this is a rare phenomenon.

The dense molecular medium in the bar region could be transported to the central region of NGC 986 within a short time scale (∼ a dynamical time scale) due to the strong shock along the bar (e.g., see Wada & Habe 1992 and references therein). This could be a major reason why we hardly observe such a gas-rich bar in galaxies (e.g., Hüttemeister et al. 1999). Therefore, the discovered dense gas bar in NGC 986 must be a huge reservoir of possible "fuel" for future starbursts in the central region, and we suggest that the star formation process in the central region of NGC 986 could still be in a growing phase.

References

Aalto, S., Johansson, L. E. B., Booth, R. S., & Black, J. H. 1991, A&A, 249, 323

Aalto, S., Booth, R. S., Black, J. H., & Johansson, L. E. B. 1995, A&A, 300, 369

Bayet, E., Gerin, M., Phillips, T. G., & Contursi, A. 2006, A&A, 460, 467

Buta, R. 1995, ApJS, 96, 39

Crosthwaite, L. P., Turner, J. L., Buchholz, L., Ho, P. T. P., & Martin, R. N. 2002, AJ, 123, 1892

Dale, D. A., et al. 2000, AJ, 120, 583

Dame, T. M., Hartmann, D., & Thaddeus, P. 2001, ApJ, 547, 792

Devereux, N., Taniguchi, Y., Sanders, D. B., Nakai, N., & Young, J. S. 1994, AJ, 107, 2006

de Vaucouleurs, G., de Vaucouleurs, A., Corwin, H. G., Buta, R. J., Paturel, G., & Fouque, P. 1991, Third Reference Catalogue of Bright Galaxies (New York: Springer-Verlag) (RC3)

Downes, D., Reynaud, D., Solomon, P. M., & Radford, S. J. E. 1996, ApJ, 461, 186

Dumke, M., Nieten, Ch., Thuma, G., Wielebinski, R., & Walsh, W. 2001, A&A, 373, 853

Elfhag, T., Booth, R. S., Hoeglund, B., Johansson, L. E. B., & Sandqvist, A. 1996, A&AS, 115, 439

Emerson, D. T., & Graeve, R. 1988, A&A, 190, 353

Ezawa, H., Kawabe, R., Kohno, K., & Yamamoto, S. 2004, Proc of the SPIE, 5489, 763

Förster Schreiber, N. M., Roussel, H., Sauvage, M., & Charmandaris, V. 2004, A&A, 419, 501

Gao, Y., & Solomon, P. M. 2004, ApJ, 606, 271

Gao, Y., & Solomon, P. M. 2004, ApJS, 152, 63

Hafok, H., & Stutzki, J. 2003, A&A, 398, 959

Hameed, S., & Devereux, N. 1999, AJ, 118, 730

Helfer, T. T., & Blitz, L. 1993, ApJ, 419, 86

Helfer, T. T., & Blitz, L. 1997, ApJ, 478, 233

Hurt, R. L., Turner, J. L., Ho, P. T. P., & Martin, R. N. 1993, ApJ, 404, 602

Hüttemeister, S., Aalto, S., & Wall, W. F. 1999, A&A, 346, 45

Iono, D., et al. 2006, PASJ, 58, 957

Israel, F. P., & Baas, F. 2001, A&A, 371, 433

Israel, F. P., & Baas, F. 2003, A&A, 404, 495

Jarrett, T. H., Chester, T., Cutri, R., Schneider, S. E., & Huchra, J. P. 2003, AJ, 125, 525

Kamazaki, T., et al. 2005, Astronomical Society of the Pacific Conference Series, 347, 533

Kawara, K., Gregory, B., & Nishida, M. 1987, ApJL, 321, L35

Kawara, K., Nishida, M., & Phillips, M. M. 1989, ApJ, 337, 230

Kohno, K., Kawabe, R., Tosaki, T., & Okumura, S. K. 1999, ApJL, 461, L29

Kohno, K., Kawabe, R., & Vila-Vilaro, B. 1999, ApJ, 511, 157

Kohno, K., Ishizuki, S., Matsushita, S., Vila-Vilaró, B., & Kawabe, R. 2003, PASJ, 55, L1

Kohno, K. 2005, ASP Conf. Ser. 344: The Cool Universe: Observing Cosmic Dawn, 344, 242

Komugi, S., et al. 2007, PASJ, 59, in press

Koopmann, R. A., & Kenney, J. D. P. 2006, ApJS, 162, 97

Kuno, N., Nakai, N., Handa, T., & Sofue, Y. 1995, PASJ, 47, 745

Kuno, N., et al. 2007, PASJ, 59, in press

Lundgren, A. A., Wiklind, T., Olofsson, H., & Rydbeck, G. 2004, A&A, 413, 505

Malhotra, S., et al. 2001, ApJ, 561, 766

Mauersberger, R., Henkel, C., Whiteoak, J. B., Chin, Y.-N., & Tieftrunk, A. R. 1996, A&A, 309, 705

Mauersberger, R., Henkel, C., Walsh, W., & Schulz, A. 1999, A&A, 341, 256

Meier, D. S., Turner, J. L., Crothwaite L. P., Beck, S. C. 2001, AJ, 121, 740

Muraoka, K., et al. 2007, PASJ, 59, in press

Oka, T., et al. 2007, PASJ, 59, in press

Roth, J., Mould, J., & Staveley-Smith, L. 1994, AJ, 108, 851

Sanders, D. B., Scoville, N. Z., Tilanus, R. P. J., Wang, Z., & Zhou, S. 1993, AIP Conf. Proc. 278: Back to the Galaxy, 278, 311

Sanders, D. B., Mazzarella, J. M., Kim, D.-C., Surace, J. A., & Soifer, B. T. 2003, AJ, 126, 1607

Sawada, T., Ikeda, N., Sunada, K., Kuno, N., Kamazaki, T., Morita, K.I., Kurono, Y., Koura, N., et al., 2008, PASJ, in press.

Sempere, M. J., Combes, F., & Casoli, F. 1995, A&A, 299, 371

Solomon, P. M., Downes, D., & Radford, S. J. E. 1992, ApJL, 387, L55

Sorai, K., Nakai, N., Kuno, N., Nishiyama, K., & Hasegawa, T. 2000, PASJ, 52, 785

Sorai, K., Sunada, K., Okumura, S. K., Tetsuro, I., Tanaka, A., Natori, K., & Onuki, H. 2000, Proc. SPIE, 4015, 86

Thornley, M. D., Schreiber, N. M. F., Lutz, D., Genzel, R., Spoon, H. W. W., Kunze, D., & Sternberg, A. 2000, ApJ, 539, 641

Tosaki, T., Shioya, Y., Kuno, N., Hasegawa, T., Nakanishi, K., Matsushita, S., & Kohno, K. 2007, PASJ, 59, 33

Tosaki, T., Miura, R., Sawada, T., Kuno, N., Nakanishi, K., Kohno, K., Okumura, S. K., & Kawabe, R. 2007, ApJL, 664, L27

Tully, R. B. 1988, Nearby Galaxies Catalogue (Cambridge: Cambridge Univ. Press)

Veron-Cetty, M.-P., & Veron, P. 1986, A&AS, 66, 335

Vila-Vilaró, B., Cepa, J., & Butner, H. M. 2003, ApJ, 594, 232

Wada, K., & Habe, A. 1992, MNRAS, 258, 82

Walsh, W., Beck, R., Thuma, G., Weiss, A., Wielebinski, R., & Dumke, M. 2002, A&A, 388, 7

Yao, L., Seaquist, E. R., Kuno, N., & Dunne, L. 2003, ApJ, 588, 771

Young, J. S., Allen, L., Kenney, J. D. P., Lesser, A., & Rownd, B. 1996, AJ, 112, 1903
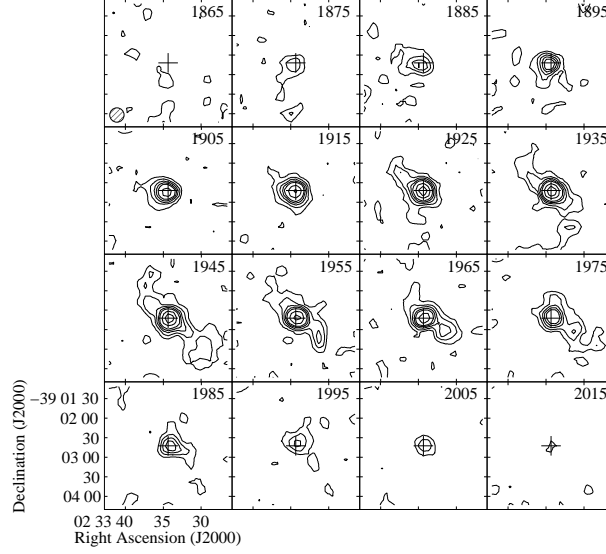
Fig. 1. Velocity channel maps of the CO(3–2) emission in NGC 986 obtained by ASTE. Contour levels are 2, 4, 6, 8, 10, 15, 20, and 25 σ, where 1 σ = 25 mK on the T_{mb} scale or 1.5 Jy beam^{-1}. Each map is labeled by the LSR velocity in km s^{-1}. The central cross in each panel indicates the position of the nucleus (defined by the peak position of the NIR continuum from 2MASS/NED).
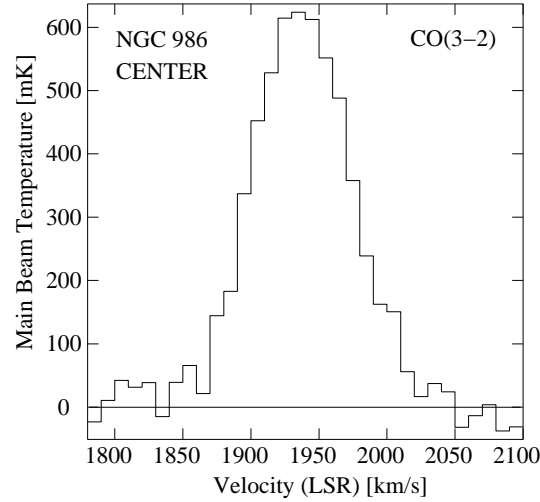
Fig. 2. ASTE CO(3–2) spectrum at the central position of NGC 986. The effective spatial resolution (see Section 2) of the spectrum is 25$''$ (HPBW). The peak temperature of approximately 0.6 K corresponds to 36 Jy beam^{-1}.

11
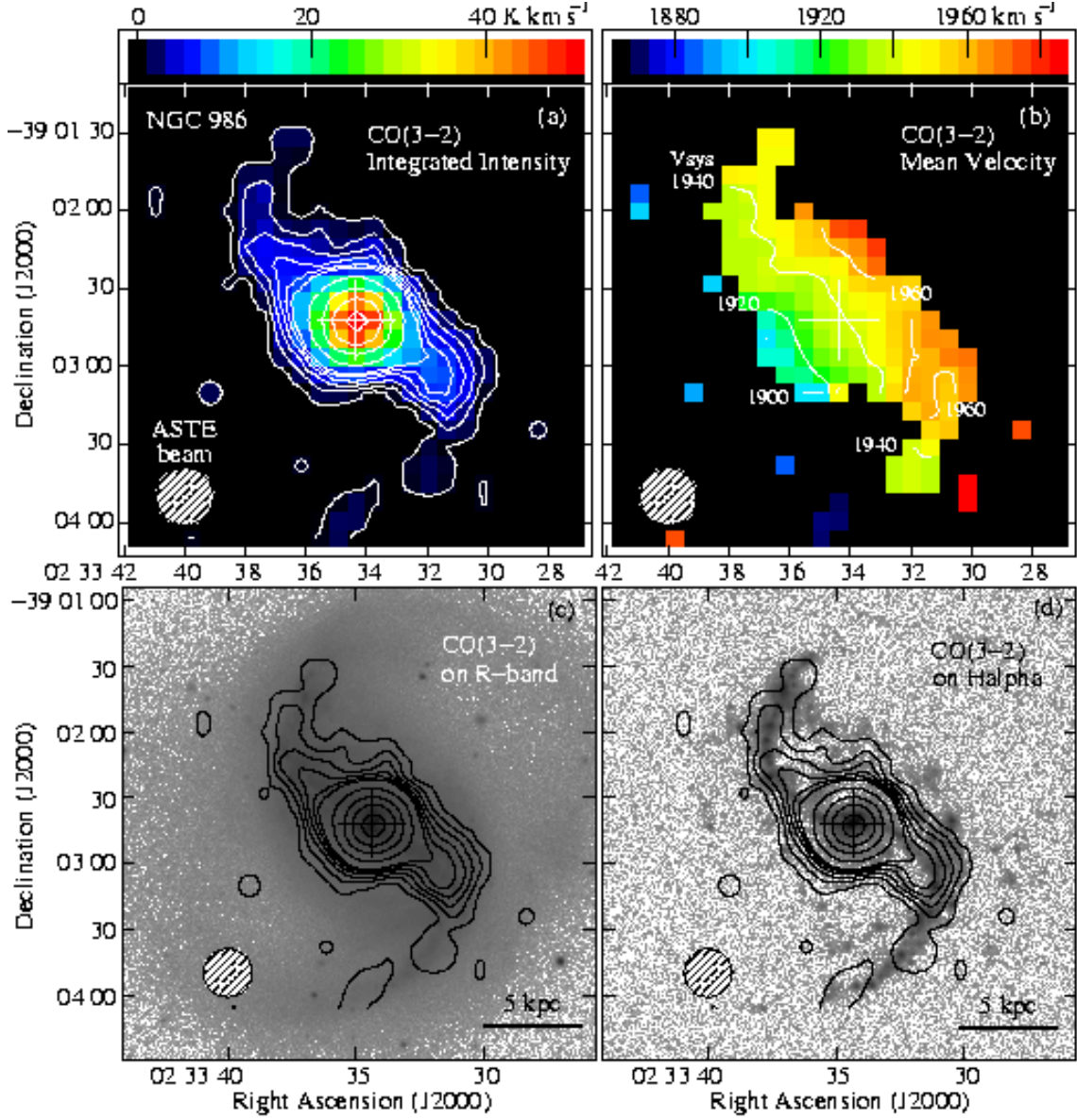
Fig. 3. (a) Velocity-integrated CO(3–2) intensity map of NGC 986, obtained by the OTF mode using the SC345 receiver mounted on ASTE. The image size is $3' \times 3'$ or 20×20 kpc at a distance of 23 Mpc. Contour levels are 1, 4, 7, 10, 13, 16, 30, 50, 70, & 90 % of the peak intensity, 55.2 K km s^{-1} or 3.35×10^3 Jy beam^{-1} km s^{-1}. The central cross indicates the position of the nucleus (defined by the peak position of the NIR continuum from 2MASS/NED). (b) Intensity-weighted mean velocity map of CO(3–2) in NGC 986. Contours are labeled by the LSR velocity. (c) Contour map of the CO(3–2) integrated intensity superposed on the R-band continuum image of NGC 986 (Hameed & Devereux 1999). (d) Contour map of the CO(3–2) integrated intensity superposed on the continuum-subtracted Hα image of NGC 986 (Hameed & Devereux 1999)

12
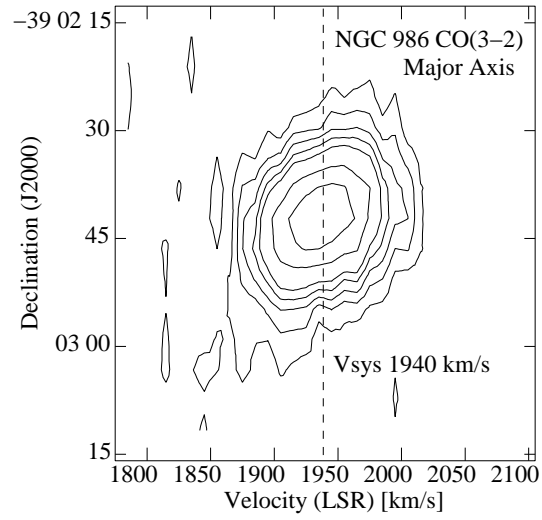
Fig. 4. ASTE CO(3–2) position-to-velocity (PV) diagram along the major axis (P.A. = 127°; Table 2) of NGC 986. Contour levels are 2, 4, 6, 8, 10, 15, 20, and 25 σ, where 1 σ = 25 mK on the T_{mb} scale or 1.5 Jy beam^{-1}.

Table 1. Sample galaxies of ADIoS project.

Object	Map size	Mode[†]	Reference	Complementary CO(1–0) data
M 83	$5' \times 5'$	PS	Muraoka et al. 2007	NRO 45 m (Kuno et al. 2007)
a GMA in M 31	$1'.5 \times 1'.5$	PS	Tosaki et al. 2007a	NRO 45 m (Tosaki et al. 2007a)
NGC 986	$3' \times 3'$	OTF	this work	—
NGC 253	$9' \times 3'$	OTF	Nakanishi et al. (in prep.)	NRO 45 m (Sorai et al. 2000a)
NGC 604 (in M33)	$5' \times 5'$	OTF	Tosaki et al. 2007b	NRO 45 m (Tosaki et al. 2007b)

[†] PS = position switching, OTF = on-the-fly mapping.

Table 2. Properties of NGC 986.

Parameter		Value	Reference
Distance		23.2 Mpc	(1)
Scale		112 pc/$''$	
Morphology		$(R'_1)SB(rs)b$	(2)
Position of nucleus	R.A.(J2000)	$02^h33^m34^s.35$	(3)
	Decl.(J2000)	$-39°02'42''.2$	
Systemic velocity (LSR)[*]		1969 km s^{-1}	(4)
		1945 km s^{-1}	(5)
		1942 ± 10 km s^{-1}	this work
Inclination (0° is face-on)		42°	(1)
		41°	(6)
		55°	(7)
		37°	this work
Position angle (from north to east)		150°	(6)
		127°	(7)
		127°	this work
Global FIR luminosity L_{FIR}		$3.5 \times 10^{10} L_\odot$	(8)
Global CO(3–2) luminosity $L'_{\mathrm{CO(3-2)}}$		$(5.4 \pm 1.1) \times 10^8$ K km s^{-1} pc^2 [†]	this work
Molecular gas mass $M(\mathrm{H_2})$		$2.6 \times 10^9 M_\odot$ [‡]	this work
Star formation efficiency $L_{\mathrm{FIR}}/M(\mathrm{H_2})$		14 $L_\odot/M_\odot$	this work
Star formation efficiency $L_{\mathrm{FIR}}/L'_{\mathrm{CO(3-2)}}$		67 $L_\odot/(\mathrm{K\ km\ s^{-1}\ pc^2})$	this work

[*] To obtain the heliocentric velocity, add 15 km s^{-1} to the velocity in LSR.

[†] The quoted error represents systematic uncertainty, mainly due to the accuracy of the main beam efficiency (20 %).

[‡] Adopting a Galactic CO-to-H$_2$ conversion factor $\alpha_{\mathrm{CO}} = 2.9\ M_\odot$ (K km s^{-1} pc^2)$^{-1}$ or $X_{\mathrm{CO}} = 1.8 \times 10^{20}$ cm^{-2} (K km s^{-1})$^{-1}$ (Dame et al. 2001) and a CO(3–2)/CO(1–0) ratio $R_{3-2/1-0}$ of 0.6 (see section 3.4).

References: (1) Tully 1988; (2) Buta 1995; (3) 2MASS EXTENDED OBJECTS, Final Release (2003)/NED; (4) HI, Roth et al. 1994; (5) CO(1–0), Elfhag et al. 1996; (6) RC3 (de Vaucouleurs et al. 1991); (7) Jarrett et al. 2003/NED; (8) Sanders et al. 2003, rescaled to the value for the distance we adopted here.

Table 3. Multi transition CO intensities at the center of NGC 986.

Transition	Integrated intensities $\int T_{\mathrm{mb}}dv$ [K km s^{-1}]	Telescope	Beam efficiency η_{mb}	Beam size [$''$]	Reference
CO(1–0)	33.4 ± 0.6	SEST 15 m	0.7	43	Aalto et al. 1991
CO(1–0)	36.2 ± 0.7	SEST 15 m	0.7	44	Elfhag et al. 1996
CO(2–1)	82.4 ± 1.2	SEST 15 m	0.5	24	Aalto et al. 1995
CO(3–2)	$55.2 \pm 1.1 \pm 11^{\dagger}$	ASTE 10 m	0.6	25	this work
CO(3–2)	$21.3 \pm 0.33 \pm 4.3^{\dagger}$	ASTE 10 m	0.6	44	this work (convolved)

		Ratio	Beam size [$''$]	[kpc]	
CO(3–2)/CO(1–0) integrated intensity ratio $R_{3-2/1-0}$		0.60 ± 0.13	44	5.0	
CO(3–2)/CO(2–1) integrated intensity ratio $R_{3-2/2-1}$		0.67 ± 0.14	25	2.8	

† the first error corresponds to the S/N of the spectrum (i.e., random error only), and the second error is obtained from the systematic error, mainly due to the accuracy of the main beam efficiency (20 %).